International Journal of Nanoelectronics and Materials
IJNeaM
ISSN 1985-5761 | E-ISSN 2232-1535

Duration and Metal Doping Effects on TiO_2 Photoanodes on the Performance of Dye-Sensitized Solar Cells

Pei-Ling Low [a,b], Gregory Soon How Thien [a], Cheikh Zakaria Eldjilali[b], Yew-Keong Sin [a,b], Mian-En Yeoh [c], Siti Khadijah Mohd Bakhori [d], Ab Rahman Marlinda [e], Kah-Yoong Chan [a,b,*]

[a]*Centre for Advanced Devices and Systems (CADS), COE for Robotics and Sensing Technologies, Multimedia University, Persiaran Multimedia, 63100 Cyberjaya, Selangor, Malaysia*
[b]*Faculty of Artificial Intelligence and Engineering, Multimedia University, Persiaran Multimedia, 63100 Cyberjaya, Selangor, Malaysia*
[c]*Infineon Technologies (Kulim) Sdn. Bhd, Kulim Hi-Tech Park, 09090, Kulim, Kedah, Malaysia*
[d]*School of Physics, Universiti Sains Malaysia, 11800, USM, Penang, Malaysia*
[e]*Nanotechnology and Catalysis Research Centre (NANOCAT), Institute for Advanced Studies, Universiti Malaya, 50603 Kuala Lumpur, Malaysia*
** Corresponding author. Tel.: +6-03-8312-5438; e-mail: kychan@mmu.edu.my*

Received 23 March 2025, Revised 1 August 2025, Accepted 11 September 2025

ABSTRACT

The TiO_2 photoanode is crucial for the photovoltaic performance of dye-sensitized solar cells (DSSCs). Notably, the improved efficiency of TiO_2 photoanodes through metal ion doping significantly depends on changes in their crystal structure, morphology, and optical properties. Therefore, this study explored the drying duration effect of hydrothermally grown TiO_2 colloids (75–120 mins) to optimize the paste for doctor-blading TiO_2 photoanodes. The analysis also investigated the impact of different 1 mol% metal dopants (Sr, Zn, Al, and Nb) on the photoanodes' crystal structure, morphology, optical properties, and DSSC efficiency. Each sample was synthesized using a modified and simplified hydrothermal strategy. The 120-min duration was then determined as the optimal drying duration for producing the highest device efficiency of 3.38% for the pristine TiO_2 photoanode. This enhancement was attributed to improved crystallinity, a more rod-like and porous morphology, and a broader absorption range into visible wavelengths. Among the metal dopants, Nb significantly improved efficiency by 6.5%. In contrast, the other dopants adversely affected performance compared to the pristine TiO_2 photoanode, which was related to the mixed rutile-anatase phase ratio. Consequently, this study effectively optimized TiO_2 photoanodes in DSSCs regarding drying duration and metal doping variables based on a simplified hydrothermal approach.

Keywords: *Dye-sensitized solar cell; Photoanode; TiO_2; Metal doping, Solar energy*

1. INTRODUCTION

Dye-sensitized solar cells (DSSCs) are prominent examples of third-generation solar cell technology and have garnered significant interest since their development by O'Regan and Grätzel in 1991 [1]. These devices are favored in the solar community for their simple structure, easy fabrication process, low toxicity, and cost-effectiveness. DSSCs are photoelectrochemical cells that generate electric current without long-term chemical changes in the device. The device comprises a working electrode (dye-sensitized photoanode), an electrolyte, and a counter electrode. Meanwhile, the working electrode features photosensitive dye molecules covalently bonded to a porous nanocrystalline titanium dioxide (TiO_2) thin film, which is deposited on a transparent conducting oxide (TCO) substrate, such as fluorine-doped tin oxide (FTO). The counter electrode, made of platinum (Pt)-coated FTO, is sealed with the working electrode, and a liquid electrolyte containing a redox mediator (usually iodide/triiodide, I^-/I_3^-) fills the space between these electrodes (see Figure 1). When light strikes the DSSC, the photosensitizer absorbs photons, exciting the dye molecules from their ground state to an excited state and generating electron carriers. These electrons are then injected into and diffused through the TiO_2 layer toward the FTO, traveling from the photoanode to the counter electrode through an external circuit. At the counter electrode, the electrolyte accepts these electrons, reducing I_3^- to I^- and returning the excited dye molecules to their ground state. Subsequently, I^- is oxidized back to I_3^-. This repeating redox cycle replenishes the electrons in the electrolyte, ensuring ongoing dye regeneration and completing the circuit [2-4].

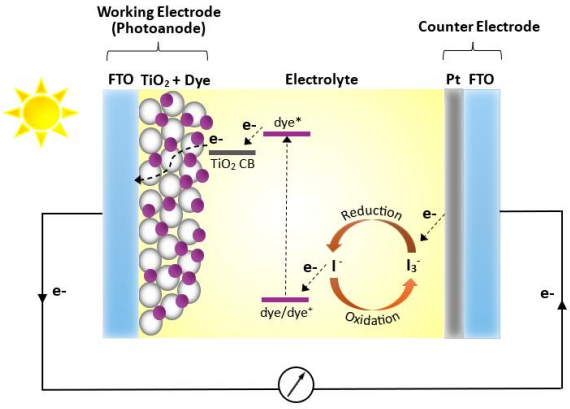

Figure 1. The DSSC device structure and operating principles

The photoanode in a DSSC consisting of dye-absorbing mesoporous TiO_2 coated on FTO is crucial for determining the device's performance. For optimal performance, the photoanode should possess the following characteristics [5, 6]:

1. High surface area for sufficient dye loading.
2. High porosity is needed for effective mass transport of dye and electrolytes.
3. Good light scattering capability for high light-harvesting efficiency (LHE).
4. A bandgap aligns with the sensitizer for efficient electron injection and rapid electron transport, minimizing charge recombination.

The conventional mesoporous TiO_2 nanoparticle-based photoanode exhibits a high surface area due to its small-sized nanoparticles. Nonetheless, this characteristic suffers from inefficient visible-range absorption due to the wide bandgap of TiO_2 (anatase: 3.2 eV; rutile: 3.0 eV), poor light scattering due to the particle size being smaller than the visible wavelength (resulting in most visible light being transmitted before absorption), high charge recombination caused by defects at the TiO_2 interface and grain boundaries, and surface states acting as trap centers in limiting charge transport [5, 7].

Various strategies have been employed to improve the structure, surface morphology, and photoelectronic properties of TiO_2-based photoanodes. These strategies include using one-dimensional (1-D) TiO_2 nanostructures, such as nanorods, nanowires, and nanotubes, to enhance charge mobility and light scattering [6-9]; incorporating carbon nanotubes (CNTs) and graphene into TiO_2 to improve conductivity, reduce charge recombination, and boost efficiency [10, 11]; and doping TiO_2 with metal ions (e.g., Cr, W, Cu, Sn, and Fe) to modify its chemical, physical, and optical properties by altering its electron transfer kinetics and band structure [12-14].

Doped-TiO_2 with metal ions has been reported to reduce the TiO_2 bandgap by introducing intermediate impurity energy levels near the conduction band, extending the absorption edge into the visible range, enhancing light absorption, and increasing free charge carriers. These changes result in improved conductivity, better electron injection efficiency, and reduced electron recombination [13, 15-18]. Additionally, metal doping can inhibit the growth rate of TiO_2 particles, leading to a larger surface area for better dye adsorption, enhanced light absorption, and increased current densities [19-22]. Although metal doping can improve device performance, certain dopants may negatively affect it by altering the crystallinity and particle size of the doped TiO_2. Therefore, further studies are necessary to fully understand how metal doping affects the structure and surface modification of TiO_2 photoanodes and their overall device performance [23].

Considering the significance of composition, size, morphology, structure, and electronic properties of modified TiO_2-based photoanodes (particularly metal doping) on DSSC performance, this process highly depends on the interactions between dopants and the TiO_2 host, specific synthesis methods, and process conditions [22, 24]. Thus, this study investigated the effects of varying the drying duration (75 to 120 mins) of hydrothermally grown TiO_2 colloids used to prepare TiO_2 paste on the photovoltaic performance of DSSCs. This time range was selected based on preliminary experiments, which showed optimal formation of paste-like TiO_2. The obtained optimal drying duration was then employed to explore the effects of various metal dopants (strontium (Sr), zinc (Zn), aluminum (Al), and niobium (Nb), applied at low concentrations, as these dopants have been consistently reported in the literature to improve the performance of modified TiO_2 photoanodes. The results demonstrated that increasing the drying duration of the TiO_2 colloids enhanced the photoanode's crystallinity, porosity, optical absorption, and overall device efficiency. Among the metal dopants tested, Nb doping demonstrated an improvement in efficiency. In contrast, other metal dopants led to reduced performance compared to the pristine TiO_2 photoanode.

2. METHODOLOGY

2.1. Materials and Methods

The materials and chemicals used in the experiments include glacial acetic acid (Friedemann Schmidt), titanium(IV) isopropoxide (TTIP, Aldrich, 97%), deionized (DI) water, strontium nitrate (EMSURE, 99%), zinc nitrate hexahydrate (Sigma-Aldrich, 98%), aluminum nitrate nonahydrate (Fluka, 98%), niobium(V) chloride (Aldrich, 99%), nitric acid (Emparta, 69%), fluorine-doped tin oxide (FTO) coated glass with an FTO thickness of 500 nm and surface resistivity of ~7 Ω/sq, acetone, isopropyl alcohol (IPA), N719 dye (Ruthenizer 535-bisTBA, Solaronix), chenodeoxycholic acid (CDCA, Solaronix), absolute ethanol, platinum (Pt) paste (Platisol T/SP, Solaronix), and iodolyte AN-50 electrolyte (Solaronix). The synthesis of TiO_2 paste and the fabrication process of DSSCs were conducted following the methods reported by Mian-En Yeoh et al. [25, 26].

2.2. Synthesis of Pristine and Metal-Doped TiO_2 Pastes

Pristine and metal-doped TiO_2 pastes were synthesized using a simplified sol-gel hydrothermal method (see Figure 2). Initially, 2.6 ml of acetic acid was added to 16.4 ml of TTIP and mixed ultrasonically for 10 mins. This mixture was then dripped into 68.4 ml of deionized (DI) water and magnetically stirred for 1 hr to initiate hydrolysis. Metal dopant precursors (Sr, Zn, Al, and Nb) at a concentration of 1 mol% were subsequently added and stirred for another 2 hrs to dope the TiO_2 (this step was omitted for the pristine TiO_2).

Approximately 2.4 ml of nitric acid was added to the mixture for peptization. The mixture was gradually heated to 80°C over the first 40 mins and maintained at this temperature for an additional 80 mins with continuous stirring. Subsequently, 25 ml of the resultant mixture was transferred into a 50 ml Teflon-lined autoclave and heated at 200°C for 10 hrs in an oven to facilitate the hydrothermal growth of the TiO_2 colloids. Approximately 0.5 ml of nitric acid was added to the colloidal solution and stirred for 15

mins. Finally, 5 ml of the colloidal solution was dried on a hotplate at 65°C for 75 to 120 mins to obtain the concentrated TiO_2 pastes.

Drying durations of 75, 90, 105, and 120 mins were used for the pristine TiO_2 colloids to assess the impact of drying time on the performance of the DSSCs. Meanwhile, metal-doped TiO_2 colloids were dried for the optimal duration of 120 mins to analyze the effects of doping on device performance, with variations only in the doping elements.

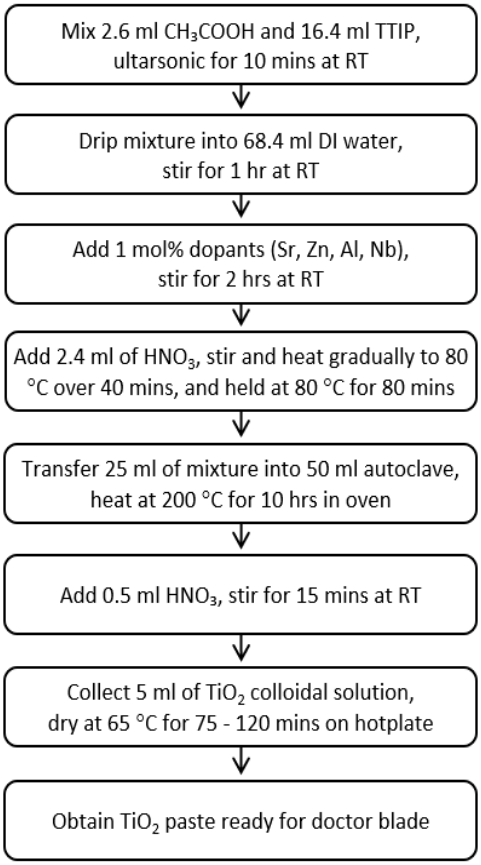

Figure 2. The flow chart of a simplified sol-gel hydrothermal synthesis process of pristine and metal-doped TiO_2 pastes

2.3. Fabrication Process of Dye-Sensitized Solar Cells

FTO substrates were precleaned ultrasonically with detergent, DI water, acetone, and isopropanol (IPA) for 15 mins each, followed by blow-drying with a nitrogen (N_2) spray gun. Figure 3 depicts that the pristine (undoped) or metal-doped TiO_2 film is deposited onto the substrate using the doctor blade technique. The TiO_2 paste prepared using the simplified hydrothermal method was then applied and annealed on a hotplate at 450°C for 30 mins. A 0.5 mM N719 dye sensitizer solution was prepared by ultrasonically mixing ruthenizer and CDCA co-adsorbent dissolved in ethanol for 10 mins. The as-prepared TiO_2 photoanode was soaked in this dye solution overnight in a dark environment for dye loading. Finally, the sensitized TiO_2 photoanode was rinsed with ethanol to remove excess dye from the surface.

Concurrently, the counter electrode was prepared by depositing a Pt film on another FTO substrate, using the doctor blade technique to apply the Pt paste, and annealed on a hotplate at 450°C for 15 mins. The DSSC device was assembled by sandwiching the TiO_2 photoanode and Pt counter electrode using binder clips and injecting the iodolyte electrolyte between the two electrodes.

2.4. Measurement and Characterization Techniques

The thickness, crystal structures, surface morphologies, elemental compositions, and optical properties of the TiO_2 photoanodes were characterized using stylus profilometer (MarSurf M 400), X-ray diffraction (XRD, PANalytical X'Pert PRO MRD PW3040/60), field-emission scanning electron microscopy (FESEM, FEI Nova NanoSEM 450), energy-dispersive X-ray spectroscopy (EDX, FEI Nova NanoSEM 450), and UV-Visible (UV-Vis) spectroscopy (Avantes AvaSpec-2048L), respectively. The photovoltaic (PV) performance of the DSSCs was measured using a solar simulator (Oriel Sol2A) under standard AM 1.5G one-sun (100 mW/cm^2) solar irradiance to obtain current-voltage (I-V) characteristics and PV parameters, including open-circuit voltage (V_{oc}), short-circuit current (I_{sc}), fill factor (FF), and efficiency (η). The PV parameters were obtained from three repeated measurements for each sample, with the reported data representing the average of these values.

3. RESULTS AND DISCUSSIONS

3.1. Effects of Drying Duration of Hydrothermal-Grown TiO_2 Colloids

Figure 4 presents the XRD patterns of pristine TiO_2 photoanodes fabricated using TiO_2 pastes prepared from hydrothermally grown TiO_2 colloids dried at 65°C for 75, 90, 105, and 120 mins. All samples displayed diffraction peaks corresponding to tin oxide (SnO_2) on FTO substrates—specifically, (110), (101), (200), (210), (211), (310), and (301) planes. Analysis of TiO_2 peaks revealed a tetragonal mixed rutile-anatase crystal structure across all samples. The anatase phase, with peaks at (101), (004), and (213), was consistent with the JCPDS standard 01-071-1166. Conversely, the predominant rutile phase exhibited prominent peaks at (110), (101), (200), (211), (220), and (301) planes (indexed following JCPDS 01-073-2224). The mixed rutile-anatase TiO_2 structure was produced from the irreversible transformation of the kinetically stable anatase phase into the thermodynamically stable rutile phase during hydrothermal treatment at elevated temperatures, with residual anatase phase remaining [27-29]. Notably, the intensities of rutile peaks [particularly in the (110), (101), and (211) directions] increased with longer drying durations from 75 to 120 mins. This outcome indicating enhanced TiO_2 crystallinity under drier conditions, significantly beyond 90 mins.

The crystallite sizes for these samples were 41.6 nm, 33.3 nm, 33.3 nm, and 46.2 nm for drying durations of 75, 90, 105, and 120 mins, respectively. These values are calculated using the rutile (110) peaks and Debye-Scherrer's formula [30] as follows:

$$D = \frac{K\lambda}{\beta \cos\theta} \quad (1)$$

where D is the crystallite size, K is a dimensionless shape factor (0.9), λ is the wavelength of Cu K_α X-ray (1.5406 Å), β

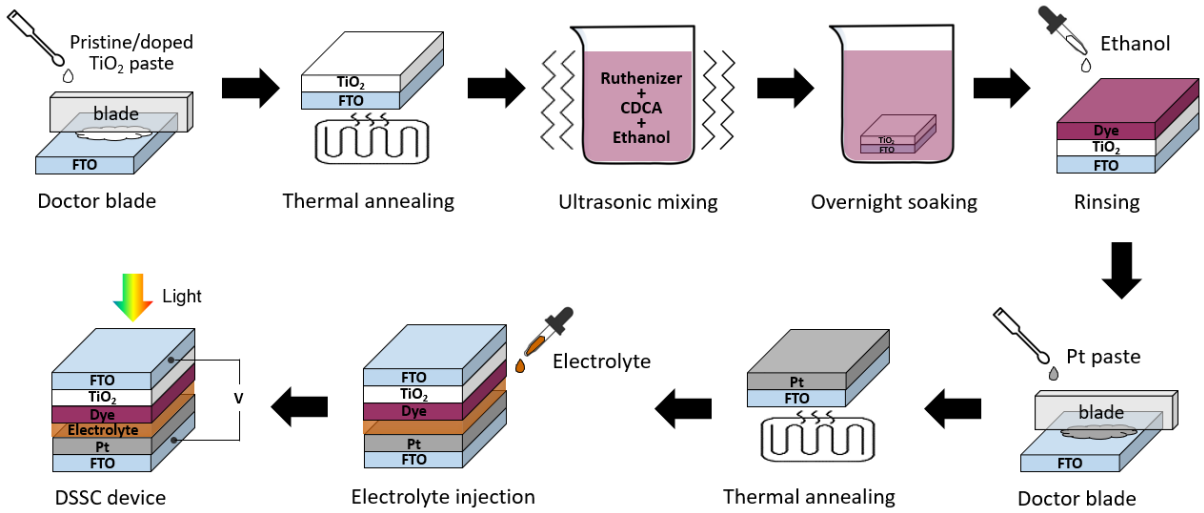

Figure 3. The schematic illustration of the fabrication process of dye-sensitized solar cells

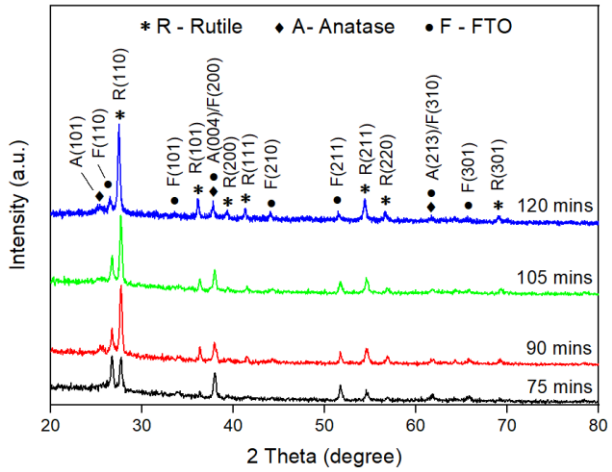

Figure 4. The XRD patterns of pristine TiO_2 photoanodes fabricated using TiO_2 pastes prepared by drying TiO_2 colloids at varying durations

is the full width at half maximum (FWHM) of the diffraction peak in radians, and θ is the Bragg's angle. Even though these results demonstrated minimal differences between 90 and 105 mins, the XRD data indicated significant mixed rutile-anatase TiO_2 phases, enhanced crystallinity, and increased grain growth for the 120-min sample.

Figure 5 illustrates the surface morphology of the TiO_2 photoanodes in the FESEM images. These images revealed aggregated nanostructures with a rod-plus-net-like morphology that uniformly covers the FTO substrate across all samples, resembling the structures reported for hydrothermally grown rutile TiO_2 nanorods [31, 32]. The morphology appeared relatively continuous for the 75-min sample, while more porous and distinct rod-like structures were observed with longer drying times (120 mins). The one-dimensional (1-D) rod-like morphology was known to provide efficient electron transport (low resistance) through nanorods and suppressed electron recombination. Thus, the porous surface structure improved the diffusion of electrolyte species around the TiO_2 film, which likely boosted the device's efficiency [6, 33, 34].

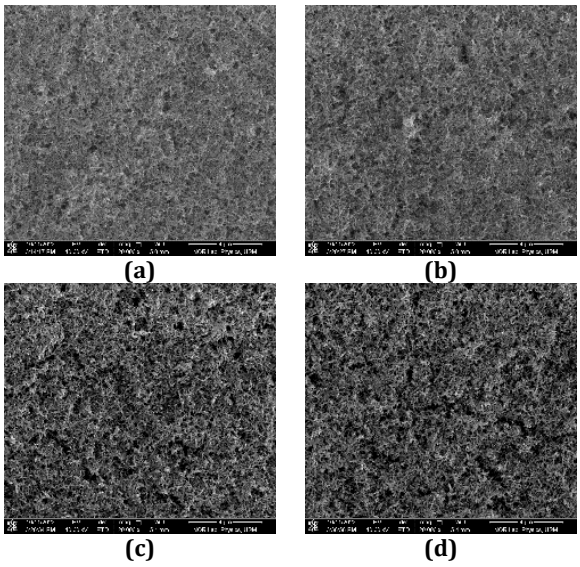

Figure 5. The 20kX-magnified FESEM images of pristine TiO_2 photoanodes fabricated using TiO_2 pastes prepared by drying TiO_2 colloids at varying durations: (a) 75 mins, (b) 90 mins, (c) 105 mins, and (d) 120 mins

Figure 6 portrays that the UV-Vis optical absorption spectra of the samples exhibit increasing peak intensities and a redshift of the primary absorption edge from 430 nm to 445 nm as the drying time progressed from 75 to 120 mins. Pure anatase TiO_2 generally exhibits intrinsic absorption at 390 nm in the ultraviolet range, with a bandgap of 3.2 eV. The observed shift to a higher absorption edge was redshifted by approximately 40 nm compared to pure anatase TiO_2. This observation suggested increased rutile content in TiO_2, which possessed a lower bandgap of 3.0 eV. Consequently, this finding supported the crystal structure noted in the XRD analysis, which yielded a dominant rutile phase with a

minor anatase component in the TiO_2 matrix [35, 36]. The extension of absorbance into the visible region with longer drying times (120 mins) also suggested enhanced visible light harvesting, which could potentially improve the efficiency of DSSCs [37, 38].

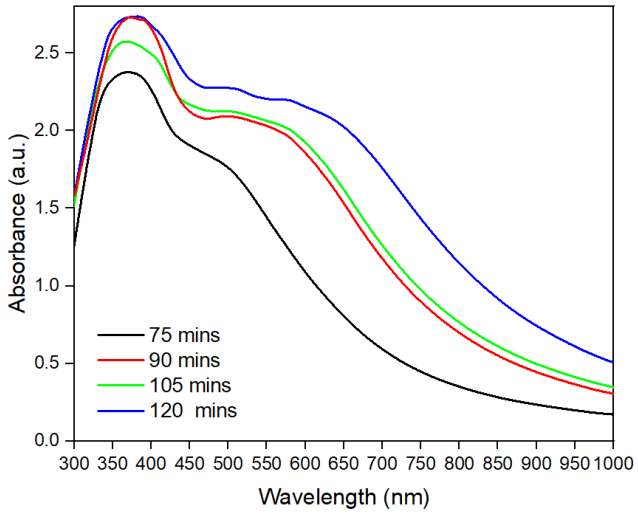

Figure 6. The UV-Vis absorption spectra of pristine TiO_2 photoanodes fabricated using TiO_2 pastes prepared by drying TiO_2 colloids at varying durations

Figure 7 and Table 1 display the *I-V* characteristic curves and photovoltaic parameters, respectively. The 120-min sample demonstrated the best photovoltaic performance, achieving the highest efficiency (η) of 3.38% and a peak short-circuit current (I_{sc}) of 12.83 mA. These results implied that the higher TiO_2 photoanode crystallinity, more porous and distinct rod-like structures, and broader optical absorption observed in the 120-min sample enhanced the DSSC performance. The performance of the 90-min and 105-min samples was also comparable and consistent with the findings from XRD patterns, crystallite sizes, and optical absorption discussed earlier.

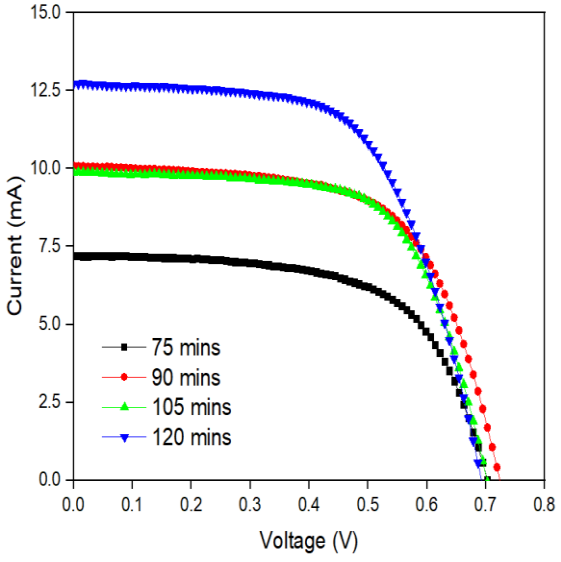

Figure 7. The *I-V* characteristic curves of DSSCs with pristine TiO_2 photoanodes fabricated using TiO_2 pastes prepared by drying TiO_2 colloids at varying durations

Table 1. Photovoltaic performance of DSSCs with pristine TiO_2 photoanodes fabricated using TiO_2 pastes prepared by drying TiO_2 colloids at varying durations

Pristine TiO_2 Drying Time (min)	**V_{oc} (V)**	**I_{sc} (mA)**	***FF***	**η (%)**
75	0.69	7.37	0.57	1.71
90	0.72	10.07	0.63	2.68
105	0.70	9.76	0.65	2.67
120	0.69	12.83	0.61	3.38

Moreover, a closer examination of the open-circuit voltage (V_{oc}) and I_{sc} trends for varying drying times revealed a trade-off between these two parameters. The I_{sc} increases while V_{oc} decreases, which possibly indicates substantial carrier recombination resulting from increased photocurrent generation. One possible reason for the simultaneous increase in both photocurrent and carrier recombination could be linked to a more porous surface structure (as observed in the 120-min sample). A higher surface porosity allows greater dye loading, thereby enhancing the photocurrent and I_{sc}. However, it also introduces more defects and surface states that exacerbate carrier recombination, thus reducing V_{oc} [39, 40]. Furthermore, the high I_{sc} coupled with a lower fill factor (*FF*) in the 120-min sample, resulting from extended drying compared to the others, may be attributed to partial internal densification within the TiO_2 photoanode. This structural compaction limits electron transport pathways and reduces electrolyte infiltration, thereby increasing series resistance and impeding efficient charge extraction [41].

Therefore, based on the highest efficiency among all samples, a 120-min drying time at 65°C for hydrothermally grown TiO_2 colloids was identified as the optimal condition for preparing TiO_2 paste using the method described in Section 2.2.

3.2. Effects of Metal Doping of TiO_2 Photoanodes

The impact of metal doping on TiO_2 photoanode and device performance was analyzed using the optimal drying duration of 120 mins to prepare both pristine and metal-doped TiO_2 pastes. The thickness of the deposited TiO_2 photoanodes was determined to be approximately 4.5 µm on average. Figure 8 presents FESEM images showing that all samples [pristine and metal-doped TiO_2 photoanodes (Sr, Zn, Al, and Nb at a concentration of 1 mol%)] exhibited a rod-plus-net-like and porous surface structure. This result was consistent with the observations recorded in Section 3.1. The rods had an average length of 300 nm and an average diameter of approximately 60 nm, forming a three-dimensional (3-D) net-like structure across the surface of the FTO substrate. Despite no significant differences in morphology were observed, the EDX measurements confirmed the elemental compositions and the presence of dopants in the metal-doped TiO_2 samples. The weight and atomic percentages (wt% and at%) of elements O, Ti, and the metal dopants (Sr, Zn, Al, and Nb) are detailed in Table 2. Based on the atomic percentages, the composition of the metal-doped TiO_2 samples averaged approximately

62:37:1 for Ti:O:dopant. Notably, no elements other than the main compounds were detected, indicating the high purity of the samples.

Figure 9 displays the XRD patterns for both pristine TiO_2 and metal-doped TiO_2 samples, all with a doping concentration of 1 mol%. All samples exhibited a coexistence of rutile and anatase phases, with the rutile phase predominating in the (110), (101), and (211) planes. On the contrary, a minor anatase phase was

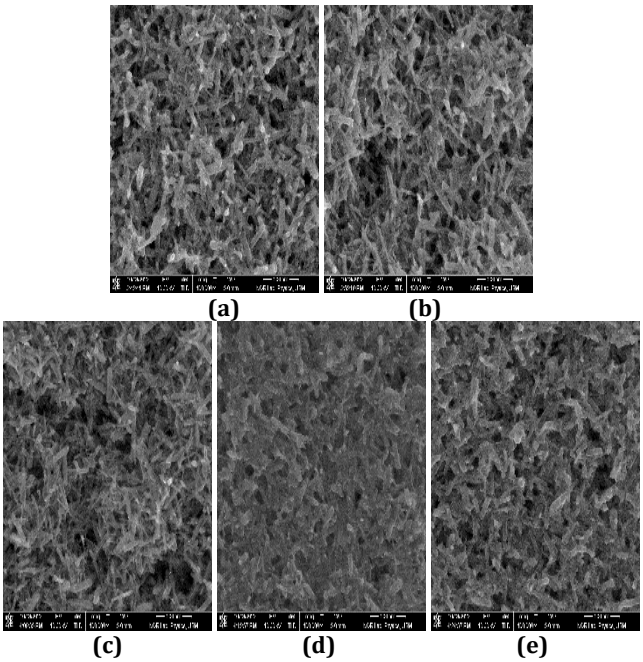

Figure 8. The 100kX FESEM images of pristine and 1 mol% metal-doped TiO_2 photoanodes: (a) undoped, (b) 1% Sr, (c) 1% Zn, (d) 1% Al, (e) 1% Nb

Table 2. Elemental analyses of 1 mol% metal-doped TiO_2 photoanodes (Sr, Zn, Al, Nb)

Samples	Element	Weight Wt %	Atomic At %
1% Sr-doped TiO_2	O	34.46	61.51
	Ti	63.36	37.78
	Sr	2.18	0.71
1% Zn-doped TiO_2	O	33.66	60.60
	Ti	63.26	38.04
	Zn	3.09	1.36
1% Al-doped TiO_2	O	37.58	63.89
	Ti	60.94	34.61
	Al	1.48	1.49
1% Nb-doped TiO_2	O	34.29	61.37
	Ti	63.46	37.93
	Nb	2.25	0.69

present in the (101), (004), and (213) orientations [42, 43]. The 1 mol% metal doping did not significantly alter the diffraction patterns, and the peaks corresponding to the dopant materials were not distinctly visible. This outcome suggested that incorporating dopant atoms into TiO_2 did not significantly change the mixed rutile-anatase crystal structure, which was consistent with similar XRD peaks observed in other reports for the same dopants at comparable concentrations [44-47].

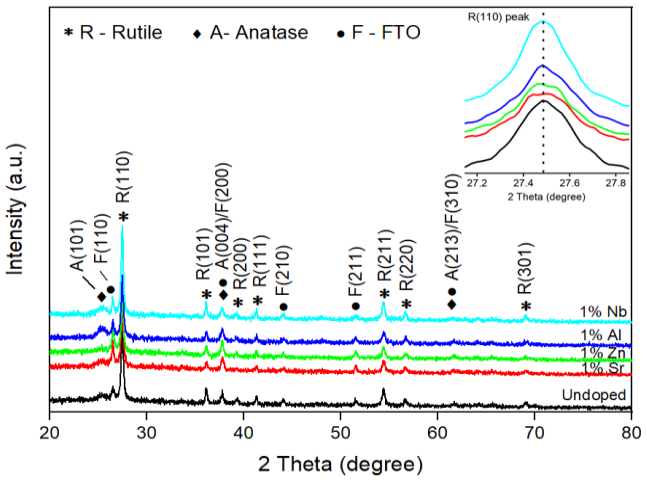

Figure 9. The XRD patterns of pristine (undoped) and 1 mol% metal-doped TiO_2 photoanodes (Sr, Zn, Al, Nb), with a close view of rutile (110) peak in the inset.

Nevertheless, a minimal peak shift was observed in the rutile (110) peak (see inset of Figure 9). The peak analyses of the rutile (110), (101), and (211) directions also revealed a slight upward shift for Zn, Al, and Sr-doped samples, while a subtle downward shift was observed for the Nb-doped TiO_2 photoanode compared to the pristine TiO_2 photoanode. These upward and downward shifts in peak positions could indicate compressive and tensile strains induced in TiO_2, respectively, due to the integration of dopant atoms into the TiO_2 lattice. Such strains were likely associated with the differing ionic radii of the dopants, smaller or larger than that of the Ti^{4+}, which affected the lattice constant of the host material [48, 49].

Table 3 presents the rutile (110) and anatase (101) phase compositions in the TiO_2 photoanodes. These values were calculated using the Spurr-Myers equation provided in Equations 2 and 3, respectively, as follows [50, 51]:

$$\%_{Rutile} = \frac{100}{1 + 0.8\left[\frac{I_A(101)}{I_R(110)}\right]} \quad (2)$$

$$\%_{Anatase} = \frac{100}{1 + 1.265\left[\frac{I_R(110)}{I_A(101)}\right]} \quad (3)$$

where the I_R and I_A represent the peak intensities of the rutile (110) and anatase (101) planes, respectively. The results demonstrated that doping with Zn, Al, and Sr reduced the rutile phase composition relative to the anatase phase. In contrast, Nb doping increased the rutile phase composition, with 85.62% in the rutile (110) phase and 14.23% in the anatase (101) phase across all samples. Different metal dopants in TiO_2 also influenced phase transformation and altered the ratio of mixed phases. This transformation was driven by changes in oxygen vacancy levels and lattice constraints, which could either inhibit or promote structural reconstruction [52]. Although pure anatase TiO_2 is generally preferred for photovoltaic applications due to its larger bandgap, higher surface area, higher electron mobility, and slower charge recombination rate, specific studies have suggested that mixed anatase-rutile TiO_2 phases can be advantageous. In

such cases, the distinct band alignments in these mixed phases provided a more efficient pathway for interfacial charge transport, facilitating the movement of electrons from the photoexcited dye through rutile TiO_2 to anatase

Table 3. The anatase/rutile phase composition in pristine and 1 mol% metal-doped TiO_2 photoanodes

Photoanode	Phase composition (%)	
	Rutile (110) plane	Anatase (101) plane
Undoped TiO_2	84.39	15.46
1% Sr-doped TiO_2	80.46	19.35
1% Zn-doped TiO_2	80.55	19.26
1% Al-doped TiO_2	79.89	19.92
1% Nb-doped TiO_2	85.62	14.23

and ultimately to the photoanode. This process reduced electron-hole recombination and enhanced photocurrent and efficiency [53, 54].

Figure 10 depicts the optical absorption spectra of the samples, revealing intrinsic absorption edges ranging from 429 nm to 443 nm (absorption extending into the visible light region). The data indicated that 1 mol% metal doping in TiO_2 resulted in a blue shift in the absorption spectra compared to pristine TiO_2. This shift was particularly notable for samples doped with Sr, Zn, and Al, which exhibited absorption edges at 429 nm, 433 nm, and 431 nm, respectively, likely leading to reduced absorption of the solar spectrum and a detrimental effect on the short-circuit current. Nonetheless, doping with Nb resulted in an absorption edge similar to that of pristine TiO_2, occurring at approximately 443 nm.

Figure 11 presents the *I-V* characteristic curve, whereas Table 4 lists the photovoltaic parameters. The 1 mol% Nb-doped TiO_2 photoanode exhibited the highest performance, with a photoconversion efficiency (η) of 3.60% and a short-circuit current (I_{sc}) of 14.37 mA. This finding represents a 6.5% improvement in efficiency compared to the pristine TiO_2 device, which produced an efficiency of 3.38%. Even though the Nb-doped TiO_2 revealed a higher I_{sc} compared to pristine TiO_2, it possessed a slightly lower open-circuit voltage (V_{oc}) and fill factor (*FF*). Conversely, other dopants such as Sr, Zn, and Al exhibited higher V_{oc} and *FF* but generated significantly reduced I_{sc}. This led to a decrease in DSSC efficiency. Previous studies also suggested that Nb doping could positively shift the flat-band potential, improve electron injection, and enhance charge transport and conductivity in TiO_2. These characteristics increased the short-circuit current and mitigated the drop in open-circuit voltage compared to pristine TiO_2 [55, 56]. Based on these results, the superior performance of the 1 mol% Nb-doped TiO_2 was likely due to both its favorable electronic properties and a mixed rutile-anatase stoichiometry, where a higher rutile content enhanced electron mobility and increased I_{sc} compared to the other dopants.

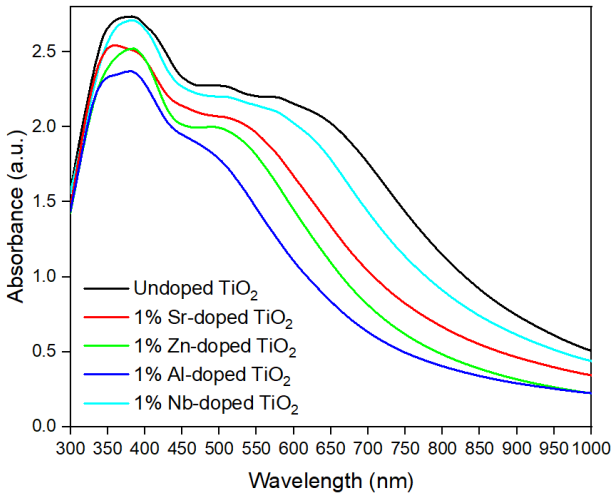

Figure 10. The UV-Vis absorption spectra of pristine (undoped) and 1 mol% metal-doped TiO_2 photoanodes (Sr, Zn, Al, Nb)

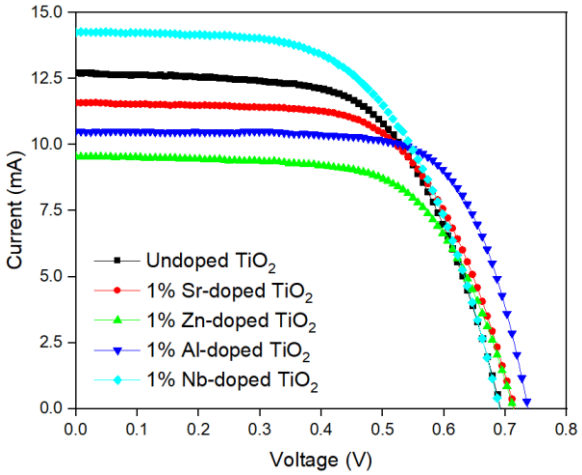

Figure 11. The *I-V* characteristics curves of pristine (undoped) and metal-doped TiO_2 photoanodes

Table 4. Photovoltaic performance of DSSCs with undoped and metal-doped TiO_2 photoanodes

Photoanode	V_{oc} (V)	I_{sc} (mA)	*FF*	η (%)
Undoped TiO_2	0.69	12.83	0.61	3.38
1% Sr-doped TiO_2	0.71	11.65	0.63	3.25
1% Zn-doped TiO_2	0.72	9.34	0.65	2.75
1% Al-doped TiO_2	0.74	10.47	0.71	3.41
1% Nb-doped TiO_2	0.68	14.37	0.59	3.60

Meanwhile, the reduced I_{sc} in Sr, Zn, and Al-doped TiO_2 suggests inefficient charge extraction and transport, possibly owing to optical absorption towards the UV region, as well as unfavorable band alignment between the dye and TiO_2. These acceptor-like dopants (Sr^{4+}, Zn^{2+}, Al^{3+}) may lower the conduction band edge, create trap states, and reduce carrier density [57]. In contrast, the donor-like Nb^{5+} dopant likely moves the Fermi level closer to the conduction band (positive flat-band potential), increasing carrier density and enhancing electron injection and overall device efficiency [56, 58].

Considering the rather similar surface morphology at the low metal doping concentration of 1 mol% for Sr, Zn, Al, and Nb compared to the pristine TiO_2 photoanode, the subtle changes observed in the XRD peak shifting, rutile–anatase phase compositions, absorption spectra, and the nature of the dopants affecting band structure indicate slight variations in the resulting device photovoltaic properties. Nevertheless, the improved performance observed with the 1 mol% Nb-doped TiO_2-based DSSC suggests that Nb doping could be a promising approach for further enhancing DSSCs to achieve even greater efficiency improvements, potentially through the optimization of doping concentration or process conditions [59, 60].

4. CONCLUSION

This study demonstrated that modifying TiO_2 photoanodes through metal doping significantly improved DSSC performance, and the synthesis process conditions strongly influence doped TiO_2. The investigations into the impact of varying the drying duration of hydrothermally grown TiO_2 colloids (75–120 mins) on the photovoltaic performance of DSSCs identified 120 mins as the optimal drying duration in producing the highest device efficiency. This improvement was attributed to the TiO_2 photoanode's higher crystallinity, distinct rod-like and porous morphology, and extended absorption range into the visible region.

Subsequently, the effects of various metal dopants (Sr, Zn, Al, and Nb) at a 1 mol% concentration on the performance of the modified TiO_2 photoanodes using this optimal drying duration were examined. The results highlighted that Nb doping enhanced efficiency by 6.5% compared to pristine TiO_2 photoanodes. This outcome was attributed to the favorable electronic properties and mixed rutile-anatase phase stoichiometry. In contrast, other dopants exhibited a detrimental impact on performance.

Overall, the findings suggest that Nb doping is promising for enhancing device performance, with further improvements potentially achievable at higher doping concentrations. Nevertheless, future studies should explore a wider range of dopant concentrations (Sr, Zn, Al, and Nb), rather than being limited to the 1 mol% concentration tested in this work, to gain an even deeper understanding of the correlation between doped TiO_2 photoanode properties and overall DSSC performance. Furthermore, long-term stability tests, which were not conducted in this study, should be included in future work to address the stability issues of DSSCs, which remain a major challenge.

ACKNOWLEDGMENTS

This research was funded by the Ministry of Higher Education (MOHE), Malaysia, under the Fundamental Research Grant Scheme (FRGS 2022-1) (Project Ref: FRGS/1/2022/TK08/MMU/03/1).

REFERENCES

[1] B. O'Regan and M. Grätzel, "A Low-Cost, High-Efficiency Solar Cell Based on Dye-Sensitized Colloidal TiO_2 Films," *Nature*, vol. 353, no. 6346, pp. 737-740, 1991.

[2] K. Sharma, V. Sharma, and S.S. Sharma, "Dye-Sensitized Solar Cells: Fundamentals and Current Status," *Nanoscale Research Letters*, vol. 13, no. 1, p. 381, 2018.

[3] A. Carella, F. Borbone, and R. Centore, "Research Progress on Photosensitizers for DSSC," *Frontiers in Chemistry*, vol. 6, 2018.

[4] O. Francis and A. Ikenna, "Review of Dye-Sensitized Solar Cell (DSSCs) Development," *Natural Science*, vol. 13, no. 12, pp. 496-509, 2021.

[5] S. C. T. Lau, J. Dayou, C. S. Sipaut, and R. F. Mansa, "Development in Photoanode Materials for High Efficiency Dye Sensitized Solar Cells," *International Journal of Renewable Energy Research*, vol. 4, no. 3, pp. 665-674, 2014.

[6] D. Joshy, S. B. Narendranath, Y. A. Ismail, and P. Periyat, "Recent Progress in One Dimensional TiO_2 Nanomaterials as Photoanode in Dye-Sensitized Solar Cells, " *Nanoscale Advances*, vol. 4, pp. 5202-5232, 2022.

[7] X. Hou, K. Aitola, and P. Lund, "TiO_2 Nanotubes for Dye-sensitized Solar Cells – A Review," *Energy Science & Engineering*, vol. 9, pp. 921-937, 2020.

[8] M. Ge, C. Cao, J. Huang, L. Shuhui, and Z. Chen, "A Review of One-Dimensional TiO_2 Nanostructured Materials for Environmental and Energy Applications," *Journal of Materials Chemistry A*, no. 4, pp. 6772-6801, 2016.

[9] P. Gnida, P. Jarka, P. Chulkin, A. Drygala, M. Libera, T. Z. Tánski, and E. Schab-Balcerzak, "Impact of TiO_2 Nanostructures on Dye-Sensitized Solar Cells Performance," *Materials*, vol. 14, no. 7, p. 1633, 2021.

[10] B. Kilic, S. Turkdogan, A. Astam, O. C. Ozer, M. Asgin, H. Cebeci, D. Urk, and S. P. Mucur, "Preparation of Carbon Nanotube/TiO_2 Mesoporous Hybrid Photoanode with Iron Pyrite (FeS_2) Thin Films Counter Electrodes for Dye-Sensitized Solar Cell," *Scientific Reports*, vol. 6, p. 27052, 2016.

[11] M. Zhu, X. Li, W. Liu, and Y. Cui, "An Investigation on the Photoelectrochemical Properties of Dye-Sensitized Solar Cells Based on Graphene-TiO_2 Composite Photoanodes," *Journal of Power Sources*, vol. 262, pp. 349-355, 2014.

[12] A. A. Awsha, S. H. Alazoumi, and B. Elhub, "A Review on the Development of TiO_2 Photoanode for Solar Applications," *Albahit Journal of Applied Sciences*, vol. 2, pp. 9-16, 2021.

[13] R. S. Dubey, S. R. Jadkar, and A. B. Bhorde, "Synthesis and Characterization of Various Doped TiO_2 Nanocrystals for Dye-Sensitized Solar Cells," *ACS Omega* , vol. 6, no. 5, pp. 3470-3482, 2021.

[14] B. Ünlü, S. Çakar, and M. Özacar, "The Effects of Metal Doped TiO_2 and Dithizone-Metal Complexes on DSSCs Performance," *Solar Energy*, vol. 166, pp. 441-449, 2018.

[15] S. Mahalingam and H. Abdullah, "Electron Transport Study of Indium Oxide as Photoanode in DSSCs: A Review," *Renewable and Sustainable Energy Reviews*, vol. 63, pp. 245-255, 2016.

[16] M. S. Ahmad, A. K. Pandey, and N. A. Rahim, "Advancements in the Development of TiO_2 Photoanodes and Its Fabrication Methods for Dye Sensitized Solar Cell (DSSC) Applications. A Review," *Renewable and Sustainable Energy Reviews*, vol. 77, pp. 89-108, 2017.

[17] L. B. Patle, V. R. Huse, and A. L. Chaudhari, "Band Edge Movement and Structural Modifications in Transition Metal Doped TiO_2 Nanocrystals for the Application of DSSC," *Materials Research Express*, vol. 4, no. 10, p. 105045, 2017.

[18] P. Das, D. Sengupta, B. Mondal, and K. Mukherjee, "A Review on Metallic Ion and Non-Metal Doped Titania and Zinc Oxide Photo-Anodes for Dye Sensitized Solar Cells," *Reviews in Advanced Sciences and Engineering*, vol. 4, no. 4, pp. 271-290, 2015.

[19] S. C. Erwine, L. Zu, M. Haftel, A. L. Efros, T. A. Kennedy, and D. J. Norris, "Doping Semiconductor Nanocrystals," *Nature*, vol. 436, no. 7047, pp. 91-94, 2005.

[20] R. Nicoli, D. Guillarme, N. Leuenberger, N. Baume, N. Robinson, M. Saugy, and J. -L. Veuthey, "Analytical Strategies for Doping Control Purposes: Needs, Challenges, and Perspectives," *Analytical Chemistry*, vol. 88, no. 1, pp. 508-523, 2016.

[21] S. K. M. Saad, A. A. Umar, M. I. A. Umar, M. Tomitori, M. Y. A. Rahman, M. M. Salleh, and M. Oyama, "Two-Dimensional, Hierarchical Ag-Doped TiO_2 Nanocatalysts: Effect of the Metal Oxidation State on the Photocatalytic Properties," *ACS Omega*, vol. 3, no. 3, pp. 2579-2587, 2018.

[22] C. Nizamudeen, R. Krishnapriya, M. S. Mozumder, A. -H. I. Mourad, and T. Ramachandran, "Photovoltaic Performance of MOF-Derived Transition Metal Doped Titania-Based Photoanodes for DSSCs," *Scientific Reports*, vol. 13, no. 1, p. 6345, 2023.

[23] A. Y. Al-Baitai, M. H. Mahmood, S. F. Abdulhussein, and S. M. Abdalhadi, "Metals Doped TiO_2 Nanoparticle as an Efficient Photoelectrode in Dye-Sensitized Solar Cells: A Review," *Nanochemistry Research*, vol. 9, no. 3, pp. 207-215, 2024.

[24] A. W. Jansons, K. M. Koskela, B. M. Crockett, and J. E. Hutchison, "Transition Metal-Doped Metal Oxide Nanocrystals: Efficient Substitutional Doping Through a Continuous Growth Process," *Chemistry of Materials*, vol. 29, 2017.

[25] M. -E. Yeoh, K. -Y. Chan, H. -Y. Wong, P. -L. Low, G. S. H. Thien, Z. -N. Ng, H. C. A. Murthy, R. Balachandran, "Hydrothermal Duration Effect on the Self-Assembled TiO_2 Photo-Anode for DSSC Application," *Optical Materials*, vol. 141, p. 113907, 2023.

[26] M. -E. Yeoh, K. -Y. Chan, H. -Y. Wong, P. -L. Low, G. S. H. Thien, Z. -N. Ng, H. C. A. Murthy, R. Balachandran, "A Novel Simplified Approach in Fabricating TiO_2 Photoanodes for Dye-Sensitized Solar Cells," *Materials Letters*, vol. 349, p. 134730, 2023.

[27] D. A. H. Hanaor and C. C. Sorrell, "Review of the Anatase to Rutile Phase Transformation," *Journal of Materials Science*, vol. 46, no. 4, pp. 855-874, 2011

[28] C. Byrne, R. Fagan, S. Hinder, D. E. McCormack, and S. C. Pillai, "New Approach of Modifying the Anatase to Rutile Transition Temperature in TiO_2 Photocatalysts," *RSC Advances*, vol. 6, no. 97, pp. 95232-95238, 2016.

[29] N. Wetchakun, B. Inceesungvorn, K. Wetchakun, and S. Phanichphant, "Influence of Calcination Temperature on Anatase to Rutile Phase Transformation in TiO_2 Nanoparticles Synthesized by the Modified Sol-Gel Method," *Materials Letters*, vol. 82, pp. 195-198, 2012.

[30] A. O. Bokuniaeva and A. S. Vorokh, "Estimation of Particle Size Using the Debye Equation and the Scherrer Formula for Polyphasic TiO_2 Powder," *Journal of Physics: Conference Series*, vol. 1410, no. 1, p. 012057, 2019.

[31] H. -S. Chen, C. Su, J. -L. Chen, T. -Y. Yang, N. M. Hsu, and W. -R. Li, "Preparation and Characterization of Pure Rutile TiO_2 Nanoparticles for Photocatalytic Study and Thin Films for Dye-Sensitized Solar Cells," *Journal of Nanomaterials*, vol. 2011, no. 1, p. 869618, 2011.

[32] T. S. Bhat, R. S. Devan, S. S. Mali, A. S. Kamble, S. A. Pawar, I. Y. Kim, Y. R. Ma, C. K. Hong, J. H. Kim, and P. S. Patil, "Photoelectrochemically Active Surfactant Free Single Step Hydrothermal Mediated Titanium Dioxide Nanorods," *Journal of Materials Science: Materials in Electronics*, vol. 25, pp. 4501-4511, 2014.

[33] Y. H. Jung, K. -H. Park, J. S. Oh, D. -H. Kim, and C. K. Hong, "Effect of TiO_2 Rutile Nanorods on the Photoelectrodes of Dye-Sensitized Solar Cells," *Nanoscale Research Letters*, vol. 8, no. 1, p. 37, 2013.

[34] V. A. González-Verjan, B. Trujillo-Navarrete, R. M. Félix-Navarro, N. J. Díaz de León, J. M. Romo-Herrera, J. C. Calva-Yáñez, J. M. Hernández-Lizalde, and E. A. Reynoso-Soto, "Effect of TiO_2 Particle and Pore Size on DSSC Efficiency," *Materials for Renewable and Sustainable Energy*, vol. 9, no. 2, p. 13, 2020.

[35] R. Cabrera, C. Sotelo-Vazquez, J. C. Bear, J. A. Darr, and I. P. Parkin, "Photocatalytic Evidence of the Rutile-to-Anatase Electron Transfer in Titania," *Advanced Materials Interfaces*, vol. 1, p. 1400069, 2014.

[36] D. Reyes-Coronado, G. Rodríguez-Gattorno, M. E. Espinosa-Pesqueira, C. Cab, R. D. Coss, and G. Oskam, "Phase-Pure TiO_2 Nanoparticles: Anatase, Brookite and Rutile," *Nanotechnology*, vol. 19, no. 14, p. 145605, 2008.

[37] K. Prabakar, M. -K. Son, D. Ludeman, and H. -J. Kim, "Visible Light Enhanced TiO_2 Thin Film Bilayer Dye Sensitized Solar Cells," *Special Section: Romanian Conference on Advanced Materials 2009*, vol. 519, no. 2, pp. 894-899, 2010.

[38] V. S. Katta, V. R. Chappidi, A. Kumar, S. Asthana, and S. S. K. Raavi, "Enriched Visible Light Absorption by

Au-Embedded Sm^{3+} Doped TiO_2 Compact Photoanode for Enhanced Dye-Sensitized Solar Cell Performance," *Physica B: Condensed Matter*, vol. 652, p. 414621, 2023.

[39] V. Dhas, S. Muduli, S. Agarkar, A. Rana, B. Hannoyer, R. Banerjee, and S. Ogale, "Enhanced DSSC Performance with High Surface Area Thin Anatase TiO_2 Nanoleaves," *Solar Energy*, vol. 85, no. 6, pp. 1213-1219, 2011.

[40] M. Sachs, E. Pastor, A. Kafizas, and J. R. Durrant, "Evaluation of Surface State Mediated Charge Recombination in Anatase and Rutile TiO_2," *The Journal of Physical Chemistry Letters*, vol. 7, no. 19, pp. 3742-3746, 2016.

[41] A. K. Chandiran, F. Sauvage, M. Casas-Cabanas, P. Comte, S. M. Zakeeruddin, and M. Graetzel, "Doping a TiO_2 Photoanode with Nb^{5+} to Enhance Transparency and Charge Collection Efficiency in Dye-Sensitized Solar Cells," *The Journal of Physical Chemistry C*, vol. 114, no. 37, 2010.

[42] A. Gordienko and A. Kaye, "Unique Pulsed-Laser Deposition Production of Anatase and Rutile TiO_2 on Al_2O_3," *Crystal Structure Theory and Applications*, vol. 7, no. 2, pp. 19-31, 2018.

[43] M. M. El-Desoky, I. Morad, M. H. Wasfy, and A. F. Mansour, "Synthesis, Structural and Electrical Properties of PVA/TiO_2 Nanocomposite Films with Different TiO_2 Phases Prepared by Sol-Gel Technique," *Journal of Materials Science Materials in Electronics*, vol. 31, pp. 17574-17584, 2020.

[44] H. F. Mehnane. C. Wang, K. K. Kondamareddy, W. Yu, W. Sun, H. Liu, S. Bai, W. Liu, S. Guo, and X. -Z. Zhao, "Hydrothermal Synthesis of TiO_2 Nanoparticles Doped with Trace Amounts of Strontium, and Their Application as Working Electrodes for Dye Sensitized Solar Cells: Tunable Electrical Properties & Enhanced Photoconversion Performance," *RSC Advances*, vol. 7, pp. 2358-2364, 2017.

[45] T. Rajaramanan, S. Shanmugaratnam, V. Gurunanthanan, Y. Shivatharsiny, D. Velauthapillai, P. Ravirajan, and M. Senthilnanthanan, "Cost Effective Solvothermal Method to Synthesize Zn-Doped TiO_2 Nanomaterials for Photovoltaic and Photocatalytic Degradation Applications," *Catalysts*, vol. 11, no. 6, pp. 690-703, 2021.

[46] M. Geetha, K. Suguna, P. M. Anbarasan, and V. Aroulmoji, "Preparation and Characterisation of Tailored TiO_2 Nanoparticles Photoanode for Dye Sensitised Solar Cells," *International Journal of Advanced Science and Engineering*, vol. 1, no. 1, pp. 1-5, 2014.

[47] N. Tsvetkov, L. Larina, J. K. Kang, and O. Shevaleevskiy, "Sol-Gel Processed TiO_2 Nanotube Photoelectrodes for Dye-Sensitized Solar Cells with Enhanced Photovoltaic Performance," *Nanomaterials*, vol. 10, no. 2, p. 296, 2020.

[48] B. Yang, D. Bogachuk, J. Suo, L. Wagner, H. Kim, J. Lim, A. Hinsch, G. Boschloo, M. K. Nazeeruddin, and A. Hagfeldt, "Strain Effects on Halide Perovskite Solar Cells," *Chemical Society Reviews*, vol. 51, pp. 7509-7530, 2022.

[49] T. Z. Liza, M. M. H. Tusher, F. Anwar, M. F. Monika, K. F. Amin, and F. N. U. Asrafuzzaman, "Effect of Ag-Doping on Morphology, Structure, Band Gap and Photocatalytic Activity of Bio-Mediated TiO_2 Nanoparticles," *Results in Materials*, vol. 22, p. 100559, 2024.

[50] R. A. Spurr and H. Myers, "Quantitative Analysis of Anatase-Rutile Mixtures with an X-Ray Diffractometer," *Analytical Chemistry* vol. 29, no. 5, pp. 760-762, 1957.

[51] M. J. Uddin, F. Cesano, A. R. Chowdhury, T. Trad, S. Cravanzola, G. Martra, L. Mino, A. Zecchina, and D. Scarano, "Surface Structure and Phase Composition of TiO_2 P25 Particles After Thermal Treatments and HF Etching," *Frontiers in Materials*, vol. 7, p. 192, 2020.

[52] D. A. H. Hanaor, G. Triani, and C. C. Sorrell, "Morphology and Photocatalytic Activity of Highly Oriented Mixed Phase Titanium Dioxide Thin Films," *Surface and Coatings Technology*, vol. 205, no. 12, pp. 3658-3664, 2011.

[53] G. Li, C. Richter, R. L. Milot, L. Cai, C. A. Schmuttenmaer, R. Crabtree, G. W. Brudvig, and V. Batista, "Synergistic Effect between Anatase and Rutile TiO_2 Nanoparticles in Dye-Sensitized Solar Cells," *Dalton Transactions*, vol. 45, no. 45, pp. 1007-85, 2009.

[54] Y. -H. Fan, C. -Y. Ho, and Y. -J. Chang, "Enhancement of Dye-Sensitized Solar Cells Efficiency Using Mixed-Phase TiO_2 Nanoparticles as Photoanode," *Scanning*, vol. 2017, no. 1, p. 9152973, 2017.

[55] S. B. Wategaonkar, V. G. Parale, R. P. Pawar, S. S. Mali, C. K. Hong, R. R. Powar, A. V. Moholkar, H. H. Park, B. M. Sargar, and R. K. Mane, "Structural, Morphological, and Optical Studies of Hydrothermally Synthesized Nb-Added TiO_2 for DSSC Application," *Ceramics International*, vol. 47, no. 18, pp. 25580-25592, 2021.

[56] E. S. Siliavka, A. V. Rudakova, T. V. Bakiev, A. A. Murashkina, P. D. Murzin, G. V. Kataeva, A. V. Emeline, and D. W. Bahnemann, "*Effect of the Heterovalent Sc^{3+} and Nb^{5+} Doping on Photoelectrochemical Behavior of Anatase TiO_2*," Catalysts, vol. 14, no. 76, 2024.

[57] B. Roose, S. Pathak, and U. Steiner, "Doping of TiO_2 for Sensitized Solar Cells," *Chemical Society Reviews*, vol. 44, pp. 8326-8349, 2015.

[58] Y. Liu, H. Ran, J. Fan, X. Zhang, J. Mao, and G. Shao, "Fabrication and Photovoltaic Performance of Niobium Doped TiO_2 Hierarchical Microspheres with Exposed {001} Facets and High Specific Surface Area," *Applied Surface Science*, vol. 410, pp. 241-248, 2017.

[59] L. Long, L. Wu, X. Yang, and X. Li, "Photoelectrochemical Performance of Nb-Doped TiO_2 Nanoparticles Fabricated by Hydrothermal Treatment of Titanate Nanotubes in Niobium Oxalate Aqueous Solution," *Journal of Materials Science & Technology*, vol. 30, no. 8, pp. 765-769, 2014.

[60] H. Su, Y. -T. Huang, Y. -H. Chang, P. Zhai, N. Y. Hau, P. C. H. Cheung, W. -T. Yeh, T. -C. Wei, and S. -P. Feng, "The Synthesis of Nb-Doped TiO_2 Nanoparticles for Improved-Performance Dye Sensitized Solar Cells," *Electrochimica Acta*, vol. 182, pp. 230-237, 2015.